Journal of African Earth Sciences 129 (2017) 45–55

Contents lists available at ScienceDirect

Journal of African Earth Sciences

journal homepage: www.elsevier.com/locate/jafrearsci

Two suites of gabbros in the Buem Structural Unit, of the Pan-African Dahomeyide orogen, southeastern Ghana: Constraints from new field and geochemical data

Daniel Kwayisi [a, *], Naa Afi Agra [a], Samuel B. Dampare [b], Daniel K. Asiedu [a], Prince O. Amponsah [a, c], Prosper M. Nude [a]

[a] University of Ghana, School of Physical and Mathematical Sciences, Department of Earth Science, P.O. Box LG 58, Legon, Accra, Ghana
[b] University of Ghana, School of Nuclear and Allied Sciences, P.O. Box LG 80, Legon, Accra, Ghana
[c] Azumah Resources Limited, P.O. Box PMB CT452, Cantonments, Accra, Ghana

ARTICLE INFO

Article history:
Received 6 June 2016
Received in revised form
16 December 2016
Accepted 22 December 2016
Available online 23 December 2016

Keywords:
Buem Structural Unit
Pan-African orogeny
Gabbro
Petrogenesis
Tectonic setting
SE Ghana

ABSTRACT

The Buem Structural Unit (BSU) of the Pan-African Dahomeyide orogenic belt, southeastern Ghana, is characterized by the occurrence of clastic and chemical sedimentary rocks, volcanic rocks and mafic-ultramafic rocks. The mafic rocks, comprising mainly gabbros occur in smaller proportion within the BSU. Representative samples of the gabbros have been analyzed petrographically and geochemically to infer their mode of emplacement, petrogenesis and tectonic setting. Two distinct gabbro types have been identified from petrography and whole-rock major and trace elements geochemistry, namely the B1 and B2 gabbros. The gabbros are generally phaneritic, holocrystalline and composed of plagioclase and clinopyronexe which have been replaced either completely or partially by sericite, chlorite and epidote. On the whole, B1 gabbros are deformed, altered, alkaline in nature, show no significant effect of crustal contamination and has affinity to OIB/E-MORB. The B2 gabbros, are relatively less deformed, subalkaline, akin to N-MORB and show arc signatures with minimal crustal contamination. The geochemical characteristics of the B1 gabbros are similar to the Buem volcanic rocks. The similarity of the B1 gabbros to the volcanic rocks may suggest a similar source and tectonic setting. Thus, the B1 gabbros may be related to rifting and emplacement at the eastern margin of the West African Craton (WAC). The effect of minimal crustal contamination and the arc nature of the B2 gabbros may suggest subduction related magmatism. Taken together, the occurrence of the gabbros may be related to rifting and subduction-collision at the eastern margin of the WAC.

1. Introduction

Understanding the origin and geodynamic evolution of the Buem Structural Unit is crucial in constraining the Pan-African orogenic event. During the main Pan-African orogenic phase, the West African Craton (WAC) was subjected to convergence on all its boundaries, from the north in the Anti-Atlas (Hefferan et al., 2000; Ennih and Liégeois, 2008), to the east along the Trans-Saharan belt (Black et al., 1979, 1994; Affaton et al., 1991; Attoh and Nude, 2008), to the south with the Rockelides and the Bassarides belts and to the west with the Mauritanides belt (Villenenve and Dallmeyer, 1987, Fig. 1a). Villeneuve and Cornée (1994); Trompette (1997) and Caby (1998) have interpreted the Pan-African mobile belts located in the southern edge of the WAC to indicate that, the southern margin of the WAC rifted (ca. 700 Ma), forming passive margins with clastics and carbonate sedimentation, which was followed by opening of an oceanic basin.

In Ghana, the Pan-African orogenic event resulted in the easterly subduction of oceanic lithosphere (Attoh, 1998; Agbossoumondé et al., 2004) and collision of the WAC with presumed exotic blocks to the east that resulted in the assemblage of Northwest Gondwana (Hoffman, 1991; Cordani et al., 2003; Tohver et al., 2006) about 650 Ma ago. In southeastern Ghana, the Pan-African Dahomeyide orogenic belt can be divided into three (3) Structural units based on age and tectonics (Fig. 1b; Attoh, 1982). The Buem Structural unit (BSU) is one of the three structural units of the Pan-

* Corresponding author.
E-mail address: dkwayisi@gmail.com (D. Kwayisi).

http://dx.doi.org/10.1016/j.jafrearsci.2016.12.018
1464-343X/

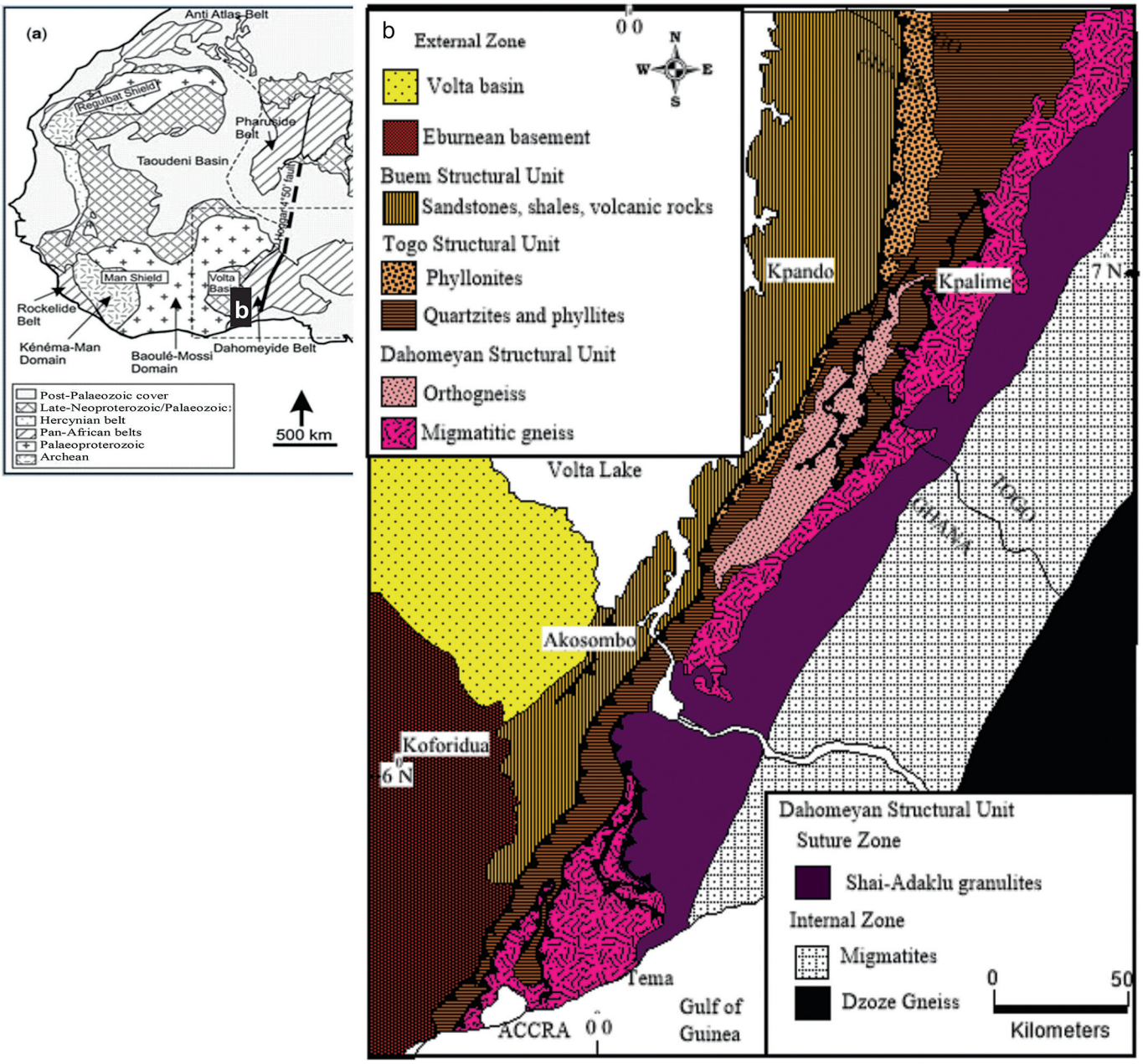

Fig. 1. (a) Simplified tectonic map of northwestern Africa showing the two main domains of the West African craton (Feybesse & Milési, 1994) (b) Map of the Dahomeyide orogen in southeastern Ghana and adjoining part of Togo (Modified from Attoh, 1990).

African Dahomeyide orogenic belts. The BSU is considered to be the youngest and the most external part of the Pan-African Dahomeyide orogenic belts (Attoh, 1982). It is bordered to the east and west by the Togo Structural Unit and the Voltaian Supergroup respectively (Fig. 1b). The BSU comprises clastic and chemical sedimentary rocks, volcanic rocks, gabbros and serpentinites (Junner, 1940; Blay, 2003; Ghana National Geological Map Project, 2009, Fig. 2).

The origin of the BSU within the Dahomeyide orogenic belts and its litho-tectonic evolution is a matter of continuous debate. Published works on the BSU have concentrated solely on the volcanics (Jones, 1990; Affaton et al., 1997; Nude et al., 2015), the sedimentary rocks (Blay, 2003; Osae et al., 2006) and the serpentinites (Asiedu et al., 2008). Published work of the Buem gabbros remains scanty in the literature. Therefore, in this paper, the petrographical and whole-rock major and trace elemental data on the Buem gabbros are presented to infer their mode of emplacement, petrogenesis and tectonic setting. The petrographic characteristics and major and trace elemental concentrations of the gabbros have been compared to the Buem volcanic rocks (Nude el al., 2015) to identify any similarities or major differences.

2. Geological setting

Rocks of the Buem Structural Unit generally strike NNE–SSW and underlie an elongated area on the eastern part of Ghana, extending northeast to the Niger River (Niger Republic), i.e. roughly 750 km long with a width of 5–50 km (Blay, 1991; Affaton et al.,

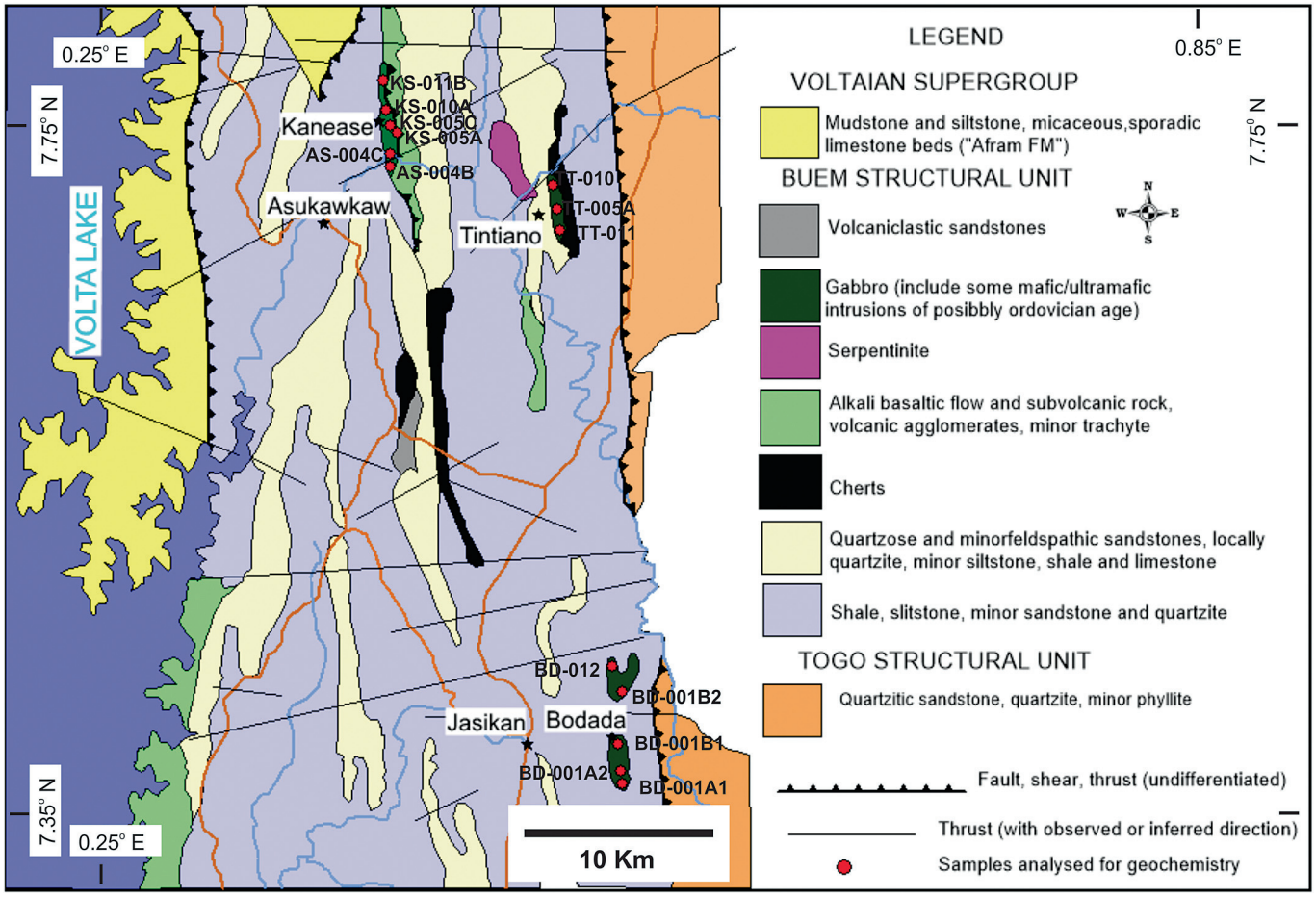

Fig. 2. Geological map of part of the Buem Structural Unit showing lithological distribution (modified from Ghana National Geological Mapping Project, 2009).

1997). The Buem units are divided into western and eastern domains, where the western domain borders the Volta basin and the eastern domain borders the Togo Structural Unit (Blay, 1991). Bell (1962) also divided the BSU into upper and lower units based on a conglomeratic unit he observed at the foot of the western flank of the Togo Plateau Massif. However, field relations show that the BSU may be subdivided into four (4) major units (Junner, 1940; Blay, 1991). They comprise sequences of clastic sediments, volcanic rocks, limestone-jasperiods and gabbros-serpentinites (Fig. 2). Variegated sandstones, wackes, jasperoids, mudstones and shale with conglomerates, and siltstones in minor quantity form the main lithologies of the clastic group. The volcanic rocks consist mainly of alkali basalts, sub-alkaline basalts, basaltic andesites, trachytes and phonolites (Nude et al., 2015) together with smaller occurrences of pyroclastic rocks and volcanic breccias. The contact between the BSU and the Togo Structural unit is marked by serpentinite and limestone. The serpentines are of two varieties; massive and schistose varieties. Griffis et al. (2002) suggested that the gabbros and serpentinites in the BSU probably represent tectonically emplaced slices of paleo-oceanic crust caught up in the suturing of adjacent continental blocks during the Pan-African orogeny.

The BSU is generally deformed; the deformation includes large-scale thrusting towards the west, folding and faulting (Attoh, 1990; Affaton et al., 1997). According to Affaton et al. (1997), the volcanic and sedimentary rocks of the BSU have been affected by extensional-related metamorphism which may have preceded the various tectonic phases of the Pan-African collision. The metamorphism in the BSU is seen as alterations in the volcanics, formation of quartz veins in the volcanic and the clastic units.

2.1. Field relation and petrography

Lithological distribution and relations are shown in Fig. 2. The gabbros outcrop mainly in the northern part particularly, in Asukawkaw, Kanease and Tintiano with minor occurrences in Bodada in the southeastern part of the area of study (Fig. 2). In Asukawkaw and Kanease, the gabbros are in tectonic contact with the volcanic rocks, where they appear schistose with calcite-quartz veinlets (Fig. 2; Fig. 3a–c). The gabbros from Asukawkaw and Kanease are generally phaneritic, granular, massive to schistose and often jointed (Fig. 3b–3d). They are composed of pyroxene, plagioclase and metallic sulphide. On the contrary, gabbros from Tintiano and Bodada are massive (Fig. 4a and b). They are however, composed mainly of plagioclase and pyroxene. Gabbros observed in Bodada intrude the shales, while those from Tintiano are associated with jasperiods (Fig. 2; Fig. 4c). The jaspers and shales appear schistose with near vertical dips (65°–70° to the SE; Fig. 4d).

Microscopically, the gabbros from Asukawkaw and Kanease are holocrystalline and composed of pyroxene and plagioclase together with abundant opaque minerals (Fig. 5a). The pyroxene has significantly been altered to hornblende, epidote and chlorite whereas the plagioclase has altered to sericite and calcite (Fig. 5a and b). These minerals also show internal cracks and fractures (Fig. 4a and b). Samples from Asukawkaw and Kanease have been cut by thin quartz-calcite veins which, have been faulted and folded

Fig. 3. Field photographs of representative rocks observed within the study area (a) Observed contact between gabbro and basalt, (b) Schistose gabbro from Asukawkaw, (c) Gabbro cut by thin veinlets of quartz and calcite, and (d) Gabbro from Asukawkaw showing well-formed joints.

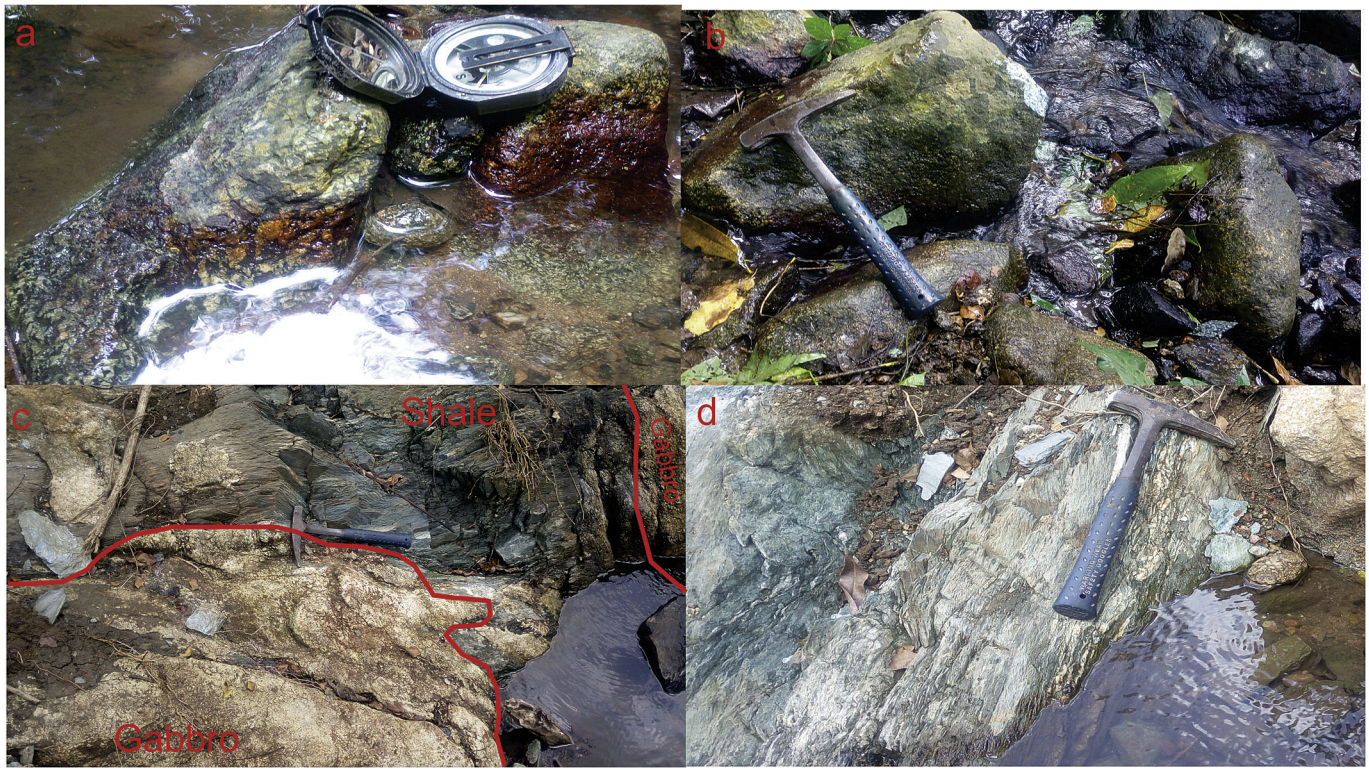

Fig. 4. Field photographs of representative rocks observed within the study area (a) and (b) Massive gabbro from Bodada, (c) Gabbro intrusion within shale, note the cross-cutting relation, observed lithologic contact between gabbro and (c) highly deformed shale with near vertical dips (65–70° to the SE direction).

(Fig. 5c and d).

Gabbros from Tintiano and Bodada in thin section are also holocrystalline, massive and composed primarily of pyroxene and plagioclase which have undergone various degrees of alterations into epidote, chlorite, sericite and opaque minerals (Fig. 6a and b). The pyroxene appears fractured in some samples. Generally,

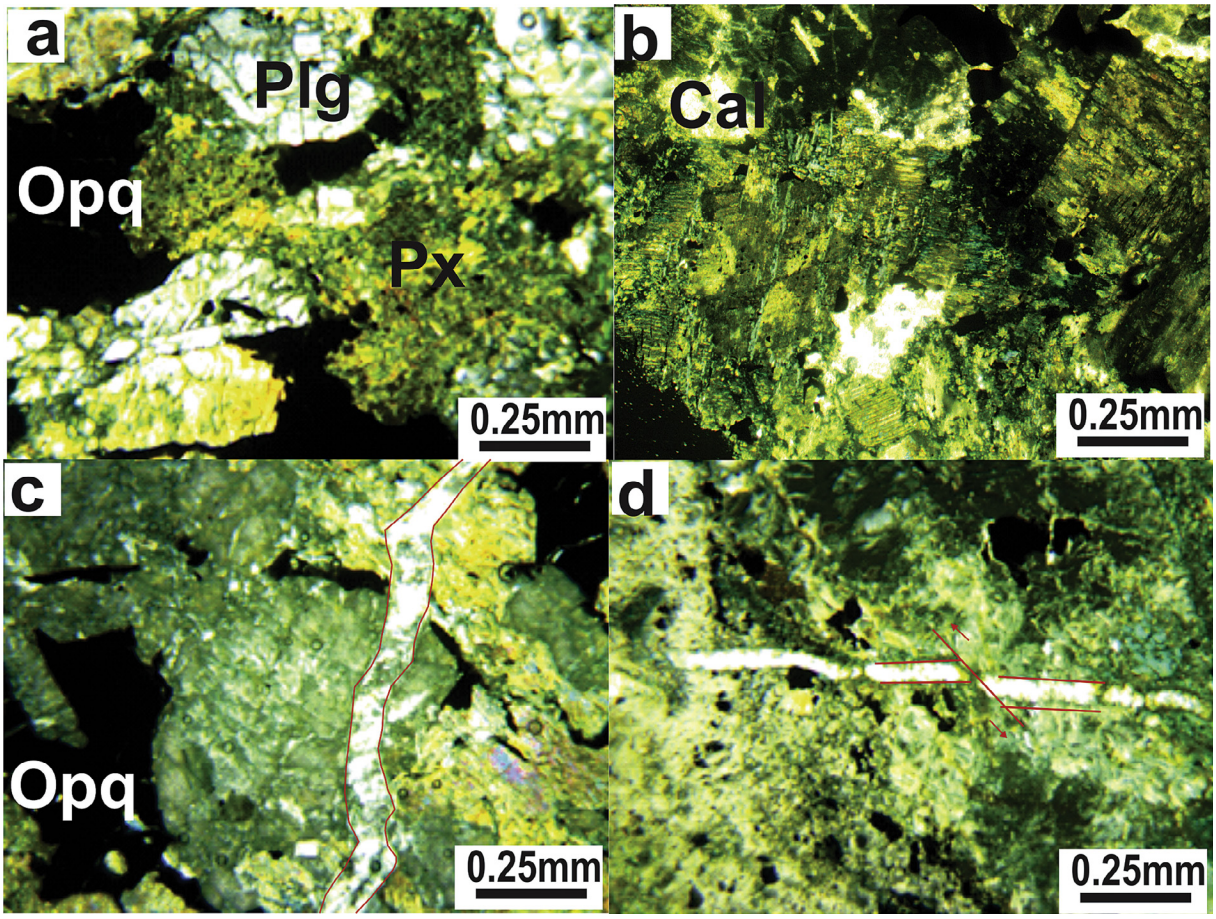

Fig. 5. Photomicrographs of mineral assemblages in the gabbros (a) Coarse grained gabbro composed of altered pyroxene (Px), plagioclase (Plg) and opaque minerals (Opq) with the plagioclase showing cracks and fractures (Crossed polars), (b) Significant alteration of plagioclase and pyroxene into chlorite, calcite and opaque minerals in gabbros from Kanease. (Crossed polars), (c) Photomicrograph of gabbro from Asukawkaw showing calcite-quartz vein that is micro-folded (Crossed polars) and (d) Micro-faulted calcite-quartz vein in gabbros from Asukawkaw (Crossed polars).

gabbros from Tintiano and Bodada are relatively less deformed than those from Asukawkaw and Kanease.

2.2. Analytical techniques

Fourteen (14) fresh and representative samples collected from Asukawkaw, Kanease, Tintiano and Bodada were sent to the ALS laboratory in Vancouver, Canada, for whole rock major and trace elements analyses. The Inductively Coupled Plasma Atomic Emission Spectrometry (ICP-AES) and Multi Elements Fusion Inductively Coupled Plasma Mass Spectrometry (ICP-MS) were used for the major and trace elements analyses respectively. Loss on Ignition (LOI) was determined at 1000 °C. Protocols observed for the analyses can be found in Nude et al. (2015). Precision is generally better than 2%.

3. Results

3.1. Major and trace element variations

Table 1 presents the whole-rock major and trace element data for the Buem gabbros. The samples show large variations in their major elements compositions. For example, SiO_2 contents range from 35.00 to 50.45 wt %, TiO_2 (0.11–8.25 wt %), Al_2O_3 (10.75–15.72 wt %), Fe_2O_3 (4.10–24.80 wt %), MgO (4.14–11.95 wt %), CaO (4.08–14.74 wt %), Na_2O (0.86–4.07 wt %) and K_2O (0.08–0.61 wt %). The gabbros from Asukawkaw and Kanease (hereafter referred to as B1 gabbros) have relatively low SiO_2, Al_2O_3, MgO and CaO and high TiO_2 and Fe_2O_3 contents than the gabbros from Tintiano and Bodada (B2 gabbros, Table 1). On the chemical classification diagram by Cox et al. (1979), the B1 gabbros plot in the alkaline field with ultrabasic composition while the B2 gabbros fall in the subalkaline field with basic composition (Fig. 7a). The B1 gabbros again plot as syeno-gabbro, syeno-diorite and nepheline syenite in Fig. 7b, supporting their alkaline nature. The B2 gabbros on the same diagram (Fig. 7b) plot as gabbro-norite and ultramafic rock, also supporting their subalkaline nature.

The gabbros are characterized by very low ∑REE contents, although slightly higher in B1 gabbros than B2 gabbros. The ∑REE contents for the B1 gabbros range from 19 to 38 ppm and that for the B2 gabbros range from 4.4 to 12.7 ppm. Both B1 and B2 gabbros on the chondrite normalized REE diagrams show depletion in LREE and flat HREE patterns similar to N-MORB with pronounced Eu positive anomalies ($Eu/Eu^* = 1.13–1.79$; Fig. 8a and b) except one B2 gabbro sample which has a weak negative Eu anomaly ($Eu/Eu^* = 0.92$). The gabbros are characterized by enriched REE concentrations than chrondrite; however, the B2 gabbros are slightly depleted in the REE contents relative to B1 gabbros and N-MORB (Fig. 8a and b). On the primitive mantle normalized diagram, the B1 gabbros depict pronounced Nb, Ta, Pb, Ti and Sr peaks and La and Ce troughs (Fig. 8c). The B2 gabbros, on the other hand, exhibit positive Ba, U and Sr peaks and negative Th, Nb, Zr and Ti anomalies

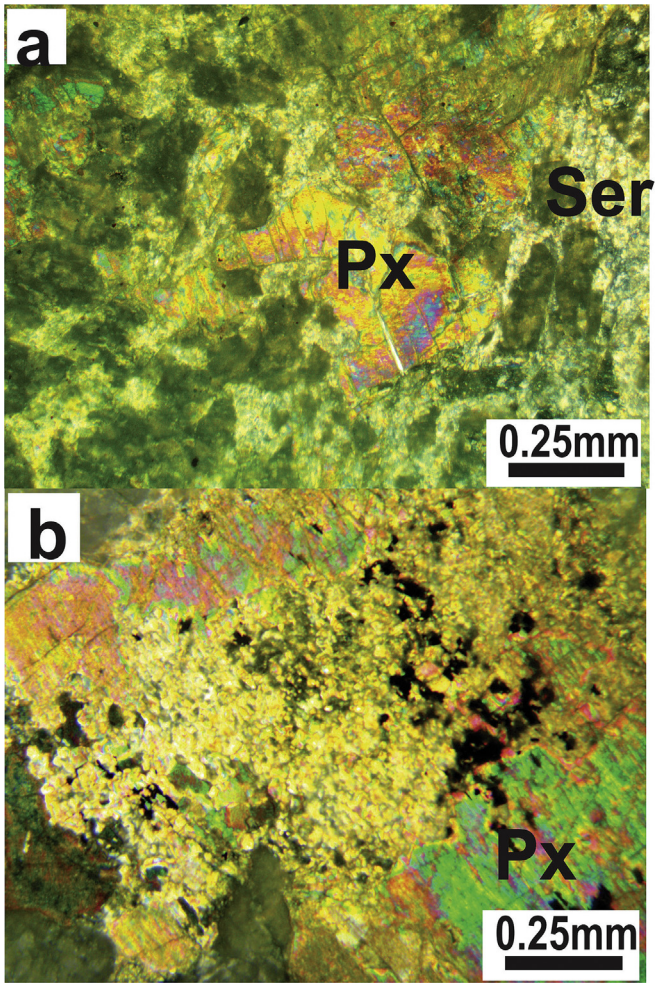

Fig. 6. (a) Photomicrograph of gabbro from bodada showing altered plagioclase and pyroxene minerals (Crossed polars) and (b) Alteration and pyroxene into opaque minerals in gabbro from Bodada (Crossed polars).

(Fig. 8d). Moreover, the B1 gabbros are enriched in the incompatible elements relative to primitive mantle with the B2 gabbros showing nearly similar incompatible elements enrichments as primitive mantle.

4. Discussion

4.1. Tectonic and emplacement implications

The B1 gabbros are in tectonic contact with the Buem volcanic rocks marked by intense shearing where the gabbros are thinly foliated, schistose and have experienced significant hydrothermal alteration with calcite-quartz veins and sulphide mineralization (Figs. 2 and 3b–d). These gabbros are deformed; well jointed, microfolded, microfaulted with cracked and fractured grains (Fig. 5–d). Thus, their occurrence at the same crustal level with the volcanic rocks, may suggest uplift to the surface.

The B2 gabbros are either associated with the jasperiods or intrude the shales (Fig. 2; Fig. 4b–d). Although they show minimal deformational features observed in thin section, their contacts with the other units are lithological not tectonic. Thus, their exposures on the surface may be due to erosion of the cover rocks.

The gabbros of the Buem Structural Unit have experienced various degrees of alteration. Therefore, in assessing their tectonic setting of emplacement, only alteration resistant elements (e.g., Nb, Zr, Ti, Y, La, Hf, Ta and Yb; Winchester and Floyd, 1977; Wood, 1980) were applied. Geochemical signatures such as Ti, Nb and Ta enrichments are characteristic of rocks derived from an E-MORB or OIB environment. However, enrichment in Ba and Th as well as depletion in Nb, Ti and Ta are characteristic of subduction-related magmas (Fitton et al., 1988; Saunders et al., 1988). Thus, the positive Ti, Nb and Ta peaks observed in the B1 gabbros on the primitive mantle diagram (Fig. 8c) may suggest their affinity for E-MORB or OIB. The negative Nb and Ti anomalies coupled with positive Ba and Th anomalies of the B2 gabbros, together with the N-MORB REE pattern and incompatible element pattern gives them an Arc/N-MORB transitional character. Their enriched LILE and flat HFSE patterns on the primitive mantle normalized multi-element diagram are similar to that of rocks derived from a subduction zone.

Jenner et al. (1991); suggested that arc gabbros have Nb/Th values < 7.5 whilst non-arc gabbros have Nb/Th values > 8.5. Transitional gabbros have Nb/Th values between 7.5 and 8.5. The B1 and B2 gabbros show affinity for non-arc and arc rocks having Nb/Th values > 8.5 and < 7.5 respectively. In the Hf–Nb–Th diagram (Fig. 9), the B1 and B2 gabbros plot in the WPA–E-MORB and IAT fields respectively, confirming their OIB–E-MORB and arc affinities.

The Buem gabbros have Ba/Ta and Ba/Nb ratios ranging from 32.6 to 128.8 and 2.59 to 7.92 for the B1 gabbros and 56–352 and 40.7–170 for the B2 gabbros respectively. The Ba/Ta and Ba/Nb values for the B1 gabbros suggest they are non-arc and were probably derived from E-MORB or OIB setting. However, the Ba/Ta and Ba/Nb ratios of the B2 gabbros suggest they were affected by orogenic processes (Pan-African orogeny) or emplaced during a subduction related event. During the Pan-African orogenic event in southeastern Ghana, there was an easterly subduction of the West African Craton (WAC) and westward movement of the Saharan Metacraton (SMC) (Attoh, 1990; Agbossomondé et al., 2004; Attoh and Nude, 2008). Hence, the B2 gabbros may have interacted with the subduction component during formation or ascent.

The geochemical signatures of the B1 gabbros are similar to that of the associated volcanic rocks (Figs. 8a, c and 9), that formed in a rifted lithospheric setting (Nude et al., 2015). The volcanic rocks are dominantly alkaline and show affinity for OIB–E-MORB with no significant effect of crustal contamination (Nude et al., 2015). Equally, the B1 gabbros are akin to OIB–E-MORB, alkaline in nature and show no significant effect of crustal contamination. Since this is similar to the volcanic rocks, similar source character and tectonic setting can be inferred. This may imply that the B1 gabbros represent mantle derived magmas in a rifted lithospheric setting.

4.2. Petrogenesis

The Buem gabbros generally define separate clusters to weak linear treads using Harker diagrams (Fig. 10). There is a general decrease in CaO, and P_2O_5 and increase in TiO_2, Al_2O_3, Na_2O and K_2O with increasing SiO_2 contents for the B1 gabbros. The B2 gabbros show decrease in MgO, CaO and increase in TiO_2, Al_2O_3, Na_2O and K_2O with increasing SiO_2 contents (Fig. 10). However, MgO, FeOt and P2O5 of the B1 and B2 gabbros on Fig. 10 appear to cluster. These features may suggest accumulation and/or weak fractional crystallization of early phases such as olivine, clinopyroxene and plagioclase. Moreover, clinopyroxene and plagioclase were observed in thin section. Minerals such as mica, apatite, titanium, ilmenite, and zircon which incorporate Na, Ti, P, K, Al during fractional crystallization were not observed in the gabbros, thus resulting in the increase of oxides of these elements with increasing SiO_2. The gabbros are albite, anorthite, diopside, hypersthene and hematite normative (Table 2), which confirm the presence of plagioclase, pyroxene and some opaque minerals observed in thin

Table 1
Major and trace element compositions of the Buem gabbros.

	B1 Gabbros						B2 Gabbros							
Sample	AS-004B	AS-004C	KS-005A	KS-005C	KS-010A	KS-011B	BD-001A1	BD-001A2	BD-001B1	BD-001B2	TT-005A	TT-010	BD-012	TT-011
Latitude	7.691°N	7.713°N	7.723°N	7.744°N	7.752°N	7.771°N	7.352°N	7.363°N	7.395°N	7.411°N	7.580°N	7.672°N	7.423°N	7.626°N
Longitude	0.361°E	0.363°E	0.404°E	0.392°E	0.373°E	0.366°E	0.501°E	0.502°E	0.511°E	0.501°E	0.472°E	0.464°E	0.512°E	0.485°E
(Wt%)														
SiO_2	39.7	35	42	39.9	42.3	40.3	50.45	50.47	49.99	49.89	46.12	48.85	49.8	49.62
TiO_2	6.28	5.09	8.21	5.98	6.2	8.25	0.27	0.27	0.29	0.27	0.11	0.24	0.38	0.35
Al_2O_3	11.9	10.75	12.33	11.64	10.75	12.1	15.72	15.36	15.52	15.57	14.03	14.61	15.19	14.76
Fe_2O_3	22.6	24.8	24.33	24.49	22.6	24.1	8.34	8.51	7.63	7.48	4.1	7.11	8.41	8.74
MgO	4.97	8.95	4.77	9.84	4.66	4.14	7.65	8.04	8.04	8.05	11.95	9.85	7.96	8.37
CaO	9.37	5.48	4.88	6.37	4.78	4.08	11.15	11.52	12.29	12.15	14.74	13.37	12.13	11.74
Na_2O	2.57	1.5	4.05	2.39	2.77	3.62	2.57	2.49	2.58	2.57	0.86	2.13	2.27	2.24
K_2O	0.19	0.02	0.51	0.61	0.09	0.48	0.15	0.09	0.12	0.11	0.02	0.07	0.09	0.11
P_2O_5	0.04	0.05	0.06	0.06	0.04	0.03	0.009	0.006	0.006	0.007	0.002	0.008	0.012	0.01
MnO	0.27	0.25	0.81	0.74	0.36	0.28	0.17	0.17	0.16	0.16	0.09	0.13	0.16	0.17
LOI	3.45	8.19	4.11	8.68	5.04	3.58	2.75	2.48	3.04	3.15	7.42	3.53	2.98	3.06
Total	101.36	100.09	102.05	99.98	99.6	100.98	99.25	99.43	99.69	99.42	99.75	99.92	99.4	99.2
(ppm)														
Cs	0.87	0.56	1.064	0.745	0.95	0.78	0.53	0.4	0.18	0.16	0.02	0.03	0.19	0.19
Rb	6.2	0.7	14.084	3.195	3.4	13.8	5.3	3	2.8	2.3	0.3	1.1	2.6	3.2
Ba	35.4	54.7	72.384	22.595	22.8	72.1	35.2	10.4	12.3	11.2	11.8	18	12.2	13.8
Th	0.22	0.2	0.24	0.23	0.19	0.22	0.22	0.05	0.07	0.05	0.05	0.05	0.05	0.05
U	0.06	0.22	0.334	0.12	0.12	0.05	0.08	0.05	0.05	0.05	0.06	0.05	0.05	0.05
Nb	8.6	10.2	9.4	8.3	8.8	9.1	0.2	0.2	0.2	0.2	0.2	0.2	0.3	0.2
Ta	0.5	0.7	0.6	0.65	0.7	0.56	0.1	0.1	0.1	0.2	0.1	0.1	0.1	0.2
K	1577	166	3984	746	747	3984	1245	747	996	913	166	581	747	913
La	2.1	2.3	1.384	1.095	1.3	1.1	0.6	0.5	0.5	0.5	0.5	0.5	0.5	0.5
Ce	5.9	6.9	3.184	3.295	3.5	2.9	3.1	0.8	1.7	0.8	0.5	1.4	1.9	1.3
Pr	0.95	1.16	0.854	0.405	0.61	0.57	0.26	0.16	0.2	0.18	0.09	0.18	0.27	0.23
Sr	169	60.4	62.284	50.395	50.6	62	105.5	101	142	128.5	56.9	108	158	136
P	174	218	131	174	174	131	39	26	26	30	8	34	52	43
Nd	5.2	7	3.784	3.195	3.4	3.5	1.4	1.1	1.2	1.1	0.5	1	1.8	1.4
Sm	1.88	2.69	1.814	1.255	1.46	1.53	0.59	0.69	0.61	0.53	0.24	0.58	0.93	0.79
Zr	67	65	68	72	66	65	2	2	3	3	2	4	5	7
Hf	2.4	2.4	2.1	2	2.2	2.3	0.3	0.3	0.3	0.2	0.2	0.3	0.4	0.4
Eu	1.18	1.33	1.26	0.58	0.78	0.98	0.44	0.39	0.42	0.39	0.15	0.31	0.44	0.38
Ti	37,648	30,514	49,459	37,168	37,169	49,458	1618	1618	1738	1618	659	1438	2278	2098
Dy	3.92	4.43	3.42	2.78	2.98	3.14	1.58	1.46	1.69	1.39	0.75	1.2	1.72	1.78
Y	20.8	24.5	17	16	16.1	16.4	8.5	8.6	9.3	8.4	3.8	7.1	11.2	10.2
Yb	2.17	2.87	2.85	1.98	1.83	2.13	0.99	1.08	1.13	1.03	0.52	0.83	1.28	1.12
Lu	0.33	0.45	0.4	0.29	0.3	0.3	0.14	0.16	0.17	0.13	0.06	0.12	0.21	0.16

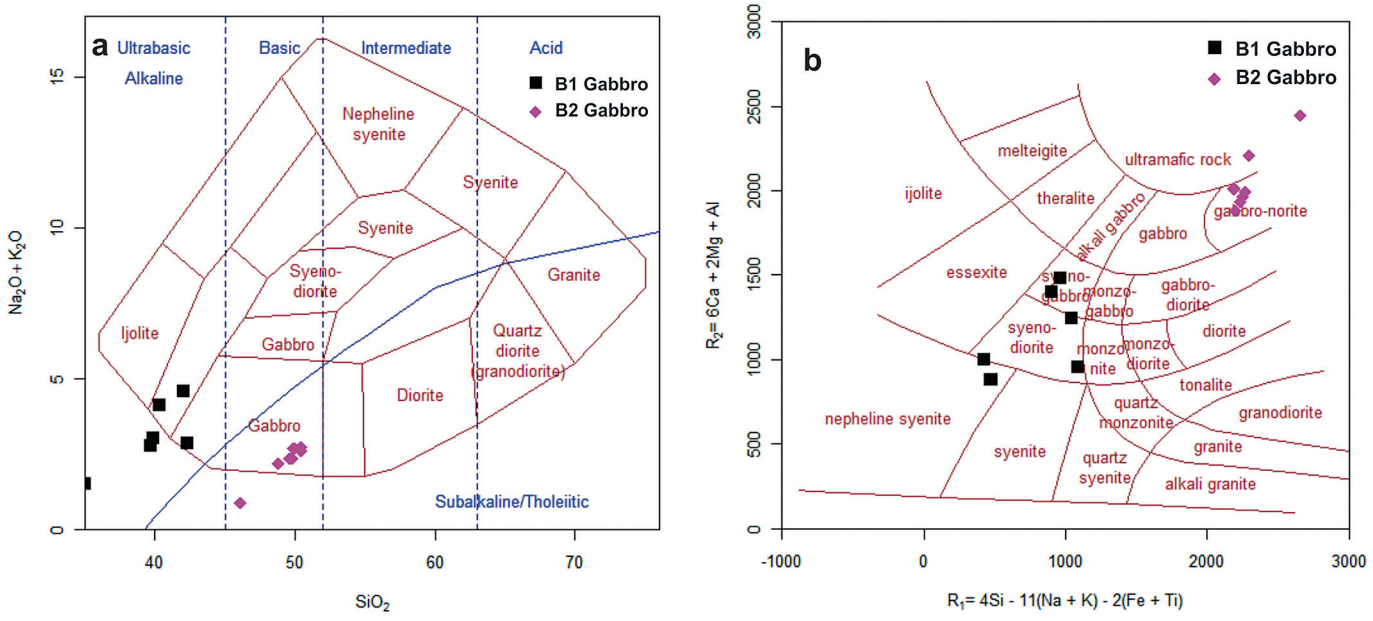

Fig. 7. Chemical classification diagrams for the Buem gabbros by (a) Cox et al. (1979) and (b) De la Roche et al. (1980).

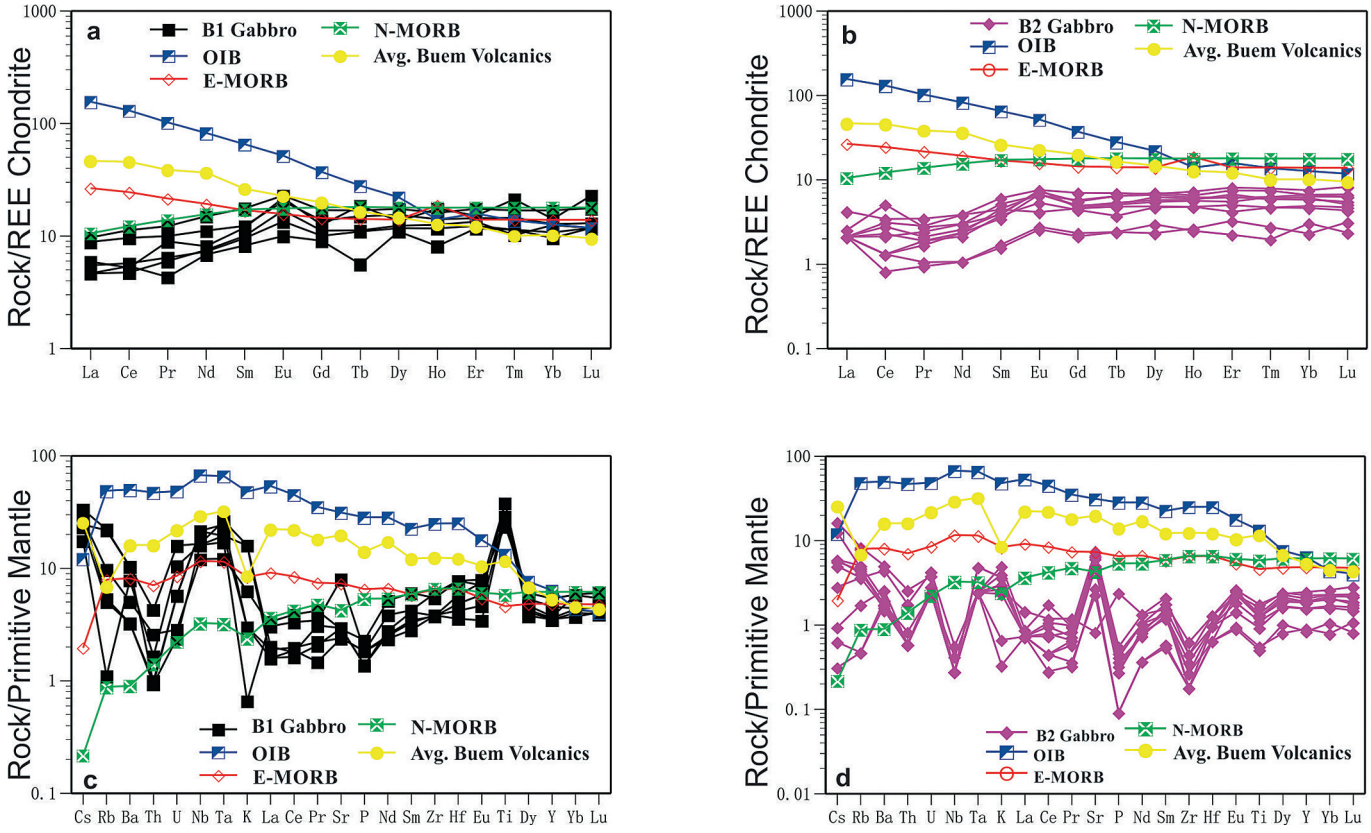

Fig. 8. REE diagrams of the gabbros normalized to REE chondrite composition of Boyton (1984) (a) B1 gabbros, (b) B2 gabbros. Primitive mantle trace element diagrams for (c) B1 gabbros and (d) B2 gabbros. Buem Volcanic data from Nude et al. (2015).

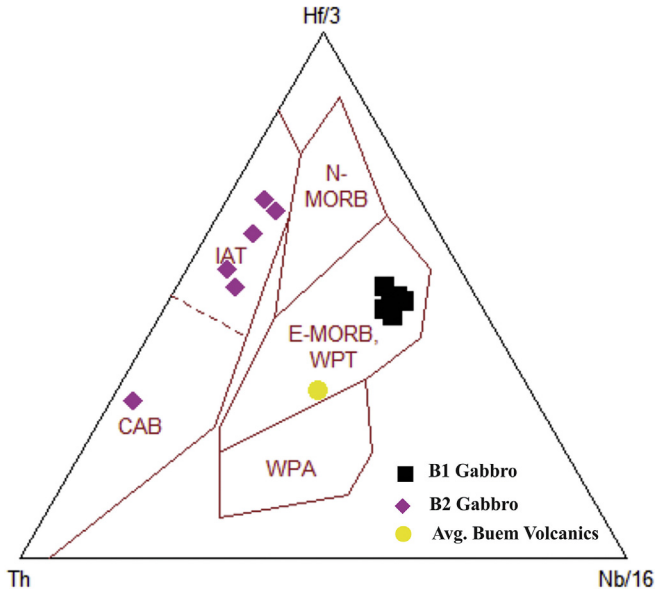

Fig. 9. Th–Hf–Nb triangular discrimination diagram of Wood (1980) for the gabbros. Buem Volcanic data from Nude et al. (2015).

section.

On the REE diagram, the LREE are depleted relative to HREE with Eu positive (Eu/Eu*) anomalies (Fig. 8a and b). The Eu positive anomalies indicate the presence of plagioclase in the rocks or mantle derived magmas. According to Marchesi et al. (2006), gabbros with strong positive Eu and Sr anomalies on their normalized trace element pattern indicate they are cumulitic rocks crystallized from mantle derived basaltic melts. In Fig. 8–d, the gabbros show strong positive Eu and Sr anomalies which are consistent with cumulitic rocks crystallized from mantle-derived basaltic melt.

Dai et al. (2011) indicated that Lu–Yb ratios are not significantly modified by partial melting or fractional crystallization. Again, mantle-derived magmas are characterized by low Lu–Yb ratios of 0.14–0.15 (Sun and McDonough, 1989). However, continental crust, according to Rudnick and Gao (2003) has relatively higher Lu–Yb ratios of 0.16–0.18. The Lu–Yb ratios for the gabbros in the study area range between 0.11 and 0.16 giving an indication that the gabbros have not been significantly affected by continental crustal contamination.

Negative Ti anomalies on the primitive mantle-normalized multi-element diagram are typical of continental crust (Rudnick and Gao, 2003). In Fig. 8c and d, the B1 and B2 gabbros show Ti positive and negative anomalies respectively, and thus suggesting there is minimal continental contribution to the magma of the B2 gabbros. Rollinson (1993) and Rudnick and Gao (2003) indicated that continental crust is rich in LREE and LILE but strongly depleted in Nb and Ta. This implies that depletion in Nb and Ta is a more diagnostic signature of continental crust (Dai et al., 2011). The B1 samples lack Nb and Ta negative anomalies (Fig. 8c) suggesting no involvement of continental crustal component. Negative Nb anomaly is characteristic of the continental crust (Rollinson, 1993) and may be an indicator of crustal involvement during the emplacement of the B2 gabbros. However, crustal rocks are also enriched in Zr, Hf, Th and U and depleted in Ta. Thus, the negative Th and Zr anomalies and the positive Ta anomaly of the B2 gabbros

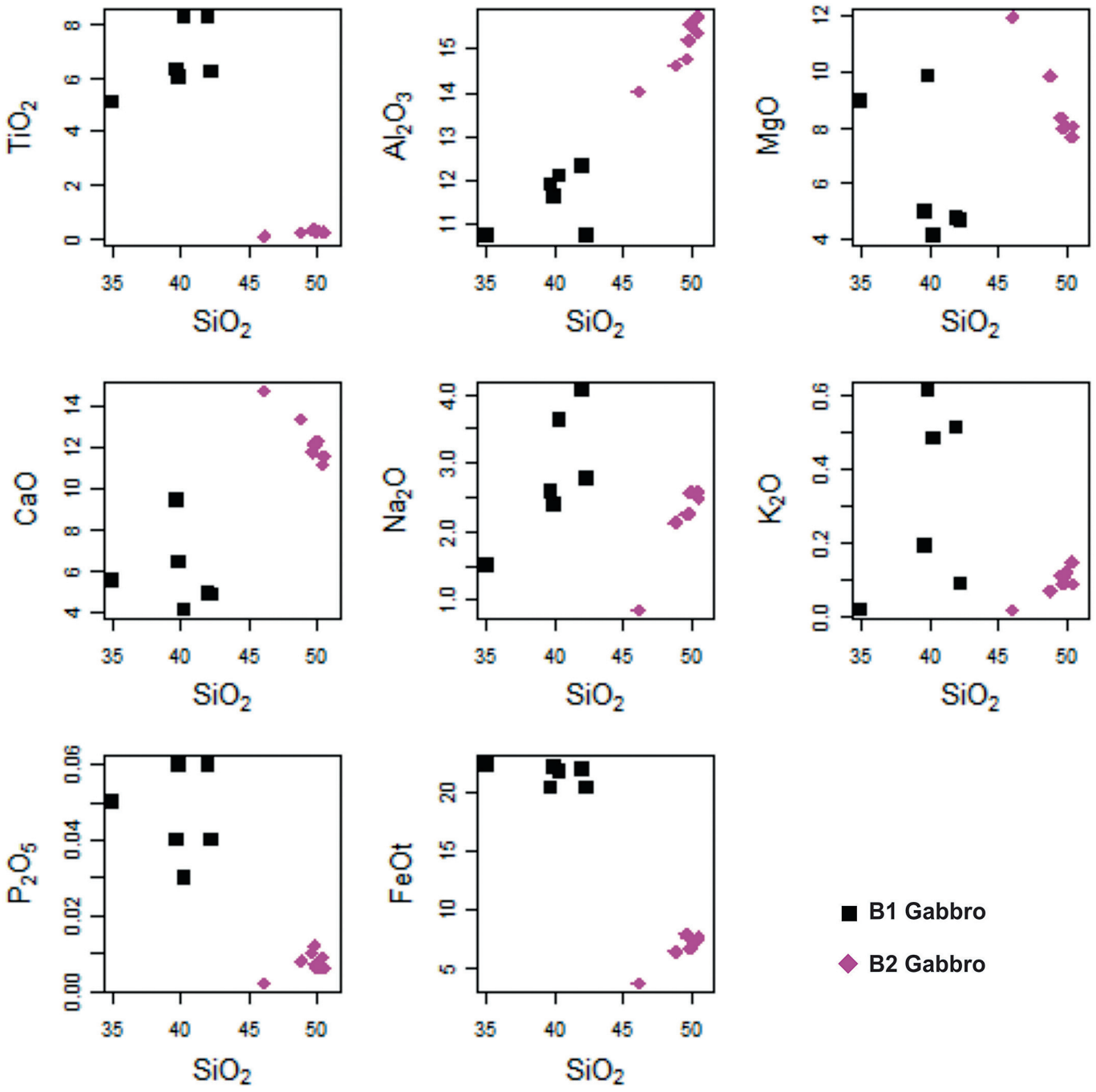

Fig. 10. SiO_2 vs major element oxides variation diagrams for the gabbros.

are inconsistent with crustal contamination. This implies that contamination in the B2 gabbros may have occurred rather at their source probably from subduction component.

Magmatic rocks derived from primary magma have MgO content >15 wt %, Mg# >65, Cr > 2000 ppm and Ni > 500 ppm (Winter 2001). With the exception of one B2 sample, the gabbros contain low MgO (<15 wt %) content, Mg# (<65), Cr < 1000 ppm, and Ni < 500 (Table 1). These imply that the gabbros were not derived from a primary magma but rather from an evolved magma. However, the MgO, Mg#, Cr and Ni contents are slightly higher for the B2 samples than B1, which may indicate that the B1 samples are relatively more evolved than B2 samples. Edwards et al. (1994), Zou et al. (2000) indicated that gabbroic rocks with high Nb and Ta may suggest an OIB/E-MORB component at the source. According to Zhou et al. (2002), typical OIB/E-MORB are enriched in Zr and Hf. Therefore, the positive Nb, Ta, Zr and Hf of the B1 gabbros may suggest the presence of an OIB/E-MORB component at their source region. Moreover, on the primitive mantle normalized diagram the B1 gabbros define trace element pattern comparable to OIB/E-MORB, however, with depleted LILE and HFSE concentrations (Fig. 8c). In addition, they display depleted LREE pattern contrary to OIB and E-MORB (Fig. 8a). Thus, to account for the very low abundance of LREE in the B1 gabbros, the source rock must have been depleted by a previously partial melting event or that, these elements must be retained at the source in residual phases such as clinopyroxene, amphibole and garnet (Wilson, 1989). The B2

Table 2
CIPW norm of the Buem Gabbros.

	B1 Gabbros						B2 Gabbros							
	AS-004B	AS-004C	KS-005A	KS-005C	KS-010A	KS-011B	BD-001A1	BD-001A2	BD-001B1	BD-001B2	TT-005A	TT-010	BD-012	BD-013
Q	2.23	2.19	1.22	0.00	10.24	3.59	4.91	4.74	2.81	2.90	0.01	0.69	4.71	4.67
Or	1.12	0.12	3.01	3.60	0.53	2.84	0.89	0.53	0.71	0.65	0.12	0.41	0.53	0.65
Ab	21.75	12.69	34.27	20.22	23.44	30.63	21.75	21.07	21.83	21.75	7.28	18.02	19.21	18.95
An	20.37	22.54	13.96	19.23	16.63	15.35	30.91	30.47	30.41	30.62	34.36	30.10	30.99	29.89
Di	3.92	0.00	0.00	0.00	0.00	0.00	18.74	20.53	23.46	22.80	30.14	27.91	22.12	21.59
Hy	10.56	22.29	11.88	18.16	11.61	10.31	10.37	10.51	9.15	9.48	15.79	11.60	9.57	10.84
Ol	0.00	0.00	0.00	4.45	0.00	0.00	0.00	0.00	0.00	0.00	0.00	0.00	0.00	0.00
Il	0.58	0.53	1.73	1.58	0.77	0.60	0.36	0.36	0.34	0.34	0.19	0.28	0.34	0.36
Hm	22.60	24.80	24.33	24.49	22.60	24.10	8.34	8.51	7.63	7.48	4.10	7.11	8.41	8.74
Tn	14.67	3.04	6.95	8.44	4.81	3.31	0.19	0.19	0.27	0.22	0.02	0.23	0.49	0.39
Ru	0.00	3.57	4.47	1.71	3.84	6.59	0.00	0.00	0.00	0.00	0.00	0.00	0.00	0.00
Ap	0.09	0.12	0.14	0.14	0.09	0.07	0.02	0.01	0.01	0.02	0.00	0.02	0.03	0.02
Sum	97.90	91.90	101.97	102.04	94.56	97.39	96.48	96.93	96.63	96.26	92.02	96.37	96.41	96.11

gabbros, on the other hand, define trace element patterns that appear similar to N-MORB with enrichment in Ba, U, and Sr and depletion in Th, Nb, Zr and Ti concentrations. Hence the B2 are akin to N-MORB with some contribution from probably subduction component.

4.3. Possible emplacement of the gabbros

Field observations and petrographical analyses have shown that the B1 gabbros are relatively more deformed than the B2 gabbro (Figs. 3 and 4). On outcrop scale, while the B1 gabbros, are well jointed and appear schistose (Fig. 3b and d) mostly at the contact with the volcanic rocks, the B2 gabbros are relatively massive (Fig. 4a and 4b). However, the jaspers and shales that are in contact with the B2 gabbros are strongly deformed (Fig. 4c and d). Again, in thin section, the B1 gabbros show various degrees of brittle-ductile deformation, with networks of veins, microfaults, microfolds, cracks and fractures. Although some of these features (cracks) can be observed in the B2 gabbros, they are not as intense as in the B1 gabbros.

Our data suggest that the B1 gabbros show petrographical and geochemical characteristics that appear similar to that of the Buem volcanic rocks, and thus similar source character and possible emplacement in the same tectonic environment may be deduced. The B2 gabbros, on the other hand, show arc character with minimal contamination from subduction component. As mentioned above, during the Pan-African orogenic event, the WAC subducted and consequently collided with the SMC. Considering all the above, the B1 gabbro might have been emplaced earlier than the B2 gabbros. The emplacement of the B1 gabbros may be linked to rifting event at the eastern margin of the WAC prior to Pan-African collision whereas the B2 gabbro may be related to the subduction and collision of the WAC with SMC. However, robust geochronological studies in required for further testing. From the above assertion, the evolution of the gabbro could possibly be as follows;

1. Rifting at the eastern margin of the WAC, followed by;
2. Extension and emplacement of the B1 gabbros at the eastern passive margin of the WAC prior to the onset of the Pan-African collision (Fig. 11a and b).
3. Subduction and collision of the WAC with the SMC and uplift of the B1 gabbros (Fig. 11c). This is followed by magma upwelling and emplacement of the B2 gabbros (Fig. 11c). Lastly, erosion and exposure of the B2 gabbros.

5. Conclusion

The petrographical and geochemical characteristics of the Buem gabbros suggest two distinct gabbros (B1 and B2). Petrographically, the constituent minerals of the B1 gabbros are highly altered and the rocks intensely deformed whereas the B2 gabbros are undeformed but highly altered. Contrary to the B1 gabbros which are alkaline with no significant crustal contamination and show OIB/E-MORB characteristics, the B2 gabbros are tholeiitic, show arc signatures and have been affected by source contamination probably from a subduction-related component. The geochemical features of the B1 gabbros indicate they likely formed within continental rift setting. Since this appears similar to the Buem volcanic rock, it suggests the emplacement of the B1 gabbros probably occurred prior to the Pan-African collision. The volcanic-arc-like nature of the B2 gabbros suggest that they were emplaced at the same time as subduction-related magmatism along the margin of the WAC just before collision with the SMC. Thus, the occurrence of the two suites of gabbros in the BSU may be related to rifting and subduction-collision at the eastern margin of the WAC.

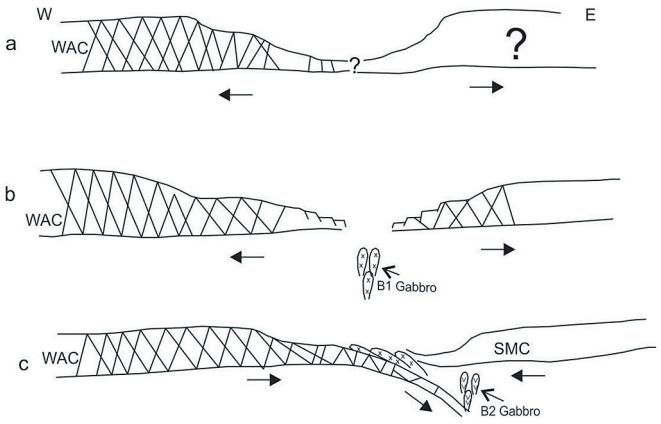

Fig. 11. Schematic diagram showing the geodynamic model of the Buem Gabbro, where WAC = West African Craton and SMC = Saharan Metacraton.

Acknowledgement

The authors acknowledge the Department of Earth Science Capacity Building Project for their financial support. Special thanks go to Damien Delvaux (Editor), Jean-Paul Liegeois (Associate Editor), Greg Shellnutt and the anonymous reviewer for their constructive comments. The authors would also like to express their gratitude to Mr. Opuni Antwi Boasiako and Asare Andrews Attuah for their assistance during the field work.

References

Affaton, P., Aguirre, L., Ménot, R.P., 1997. Thermal and geodynamic setting of the Buem volcanic rocks near Tiéle, Northwest Benin, West Africa. Precambrian Res. 82, 191–209.

Affaton, P., Rahaman, M.A., Trompette, R., Sougy, J., 1991. The Dahomeyide Orogen: tectonothermal evolution and relationships with the Volta basin. In: Dallmeyer, R.D., Lecorché, J.P. (Eds.), The West African Orogens and Circum-Atlantic Correlatives. Springer, New York, pp. 95–111.

Agbossoumondé, Y., Guillot, S., Ménot, R.P., 2004. Pan-African subduction- collision event evidenced by High-P coronas in meta-norites from the Agou Massif (southern Togo). Precambrian Res. 135, 1–21.

Asiedu, D.K., Dampare, S.B., Shibata, T., Banoeng Yakubu, B., Osae, S., 2008. The chemical composition and significance of chromian spinels in the Neoproterozoic Anum serpentinites obtained from Anum and Dake-Peki in Southeastern Ghana. J. Ghana Sci. Assoc. 10 (1), 36–43.

Attoh, K., Nude, P.M., 2008. Tectonic Significance of Carbonatite and Ultrahigh-pressure Rocks in the Pan-African Dahomeyide Suture Zone, Southeastern Ghana. Geological Society, London, pp. 217–231. Special Publications 2008, 297.

Attoh, K., 1998. High-pressure granulite facies metamorphism in the Pan-African Dahomeyide orogen, West Africa. J. Geol. 106, 236–246.

Attoh, K., 1990. Dahomeyides of Southeastern Ghana: Evidence for Oceanic Closure and Crustal Imbrication in a Pan-African Orogen. Publication occasionnelle du C.I.F.E.G., BRGM, Orleans France, 21.

Attoh, K., 1982. Structure, gravity models, and stratigraphy of an Early Proterozoic volcanic-sedimentary belt in northeastern Ghana. Precambrian Res. 18, 275–290.

Bell, S.V., 1962. Ghana Geological Survey Annual Report. Ghana Geological Survey, Accra.

Black, R., Caby, R., Moussine-Pouchkine, A., Bertrand, J.M.L., Boullier, A.M., Fabre, J., Lesquer, A., 1979. Evidence for precambrian plate tectonics in West Africa. Nature 278, 223–227.

Black, R., Latouche, L., Liégeois, J.P., Caby, R., Bertrand, J.M., 1994. Pan-African displaced terranes in the Tuareg shield (central Sahara). Geology 22, 641–644.

Blay, P., 2003. The Geology of 1/4 Feild Sheets Nos. 184, 185 and 187, Hohoe N. E., Baglo S.W. and N.W. Accra. Ghana Geological Survey Department.

Blay, P.K., 1991. Applying subduction tectonics to the evolution of the Pan-African Dahomeyide deformed belt of Ghana. In: West Africa: Proceedings of the First Local Conference on Mineral Exploration and Development and Their Impact on the Economy of Ghana, Accra, 7th December 1990. Minerals Commission Publication, pp. 52–75.

Boyton, W.V., 1984. Geochemistry of the rare-earth elements: meteorite studies. In: Henderson, P. (Ed.), Rare Earth Element Geochemistry. Elsevier, pp. 63–114.

Caby, R., 1998. Tectonic history and geodynamic evolution of northern Africa during the Neoproterozoic. In: 14 International Conference on Basement Tectonics, Ouro Preto, Abstracts, pp. 72–75.

Cordani, U.G., D'agrella-Filho, M.S., Brito-Neves, B.B., Trindale, I.F., 2003. Tearing up rodinia: the neoproterozoic paleogeography of South American cratonic fragments. Terra Nova 15, 350–359.

Cox, K.G., Bell, J.D., Pankhurst, R.J., 1979. The Interpretation of Igneous Rocks. George Allen and Unwin (Publishers), London, p. 450.

Dai, J., Wang, C., Hebert, R., Li, Y., Zhong, H., Guillaume, R., Bezard, R., Wei, Y., 2011. Late devonian OIB alkaline gabbro in the yarlung zangbo suture zone: remnants of the paleo-Tethys? Gondwana Res. 19, 232–243.

De la Roche, H., Leterrier, J., Grande Claude, P., Marchal, M., 1980. A classification of volcanic and plutonic rocks using R1-R2 diagrams and major element analyses – its relationships and current nomenclature. Chem. Geol. 29, 183–210.

Edwards, C.M.H., Menzies, M.A., Thirlwall, M.F., Morris, J.D., Leeman, W.P., Harmon, R.S., 1994. The transition to potassic alkaline volcanism in island arcs: the Ringgit-Beser complex, east Java, Indonesia. J. Petrol. 35, 1557–1595.

Ennih, N., Liégeois, J.P., 2008. The boundaries of West Africa craton, with a special reference to the basement of the Moroccan metacratonic Anti-Atlas belt. In: Ennih, N., Liégeois, J. p. (Eds.), The Boundaries of West Africa Craton. Geological Society, London, pp. 1–17 special publication, 297.

Feybesse, J.L., Milési, J.P., 1994. The Archean/proterozoic contact zone in West Africa: a mountain belt of décollement thrusting and folding on a continental margin related to 2.1 Ga convergence of Archean cratons? Precambrian Res. 69, 199–227.

Fitton, J.G., James, D., Kempton, P.D., Ormerod, D.S., Leeman, W.P., 1988. The role of lithospheric mantle in the generation of Late Cenozoic basic magmas in the western United States. J. Petrol. 331–349 (Special Lithosphere Issue).

Ghana National Geological Mapping Project, 2009. Geological Map of Ghana 1:1 000 000. Geological Survey Department of Ghana (GSD).

Griffis, R.J., Barning, K., Agezo, F.L., Akosah, F.K., 2002. Gold Deposits of Ghana. Minerals Commission, Accra, Ghana.

Hefferan, K.P., Admou, H., Karson, J.A., Saquaque, A., 2000. Anti-atlas (Morocco) role in neoproterozoic western Gondwana reconstruction. Precambrian Res. 103, 89–96.

Hoffman, P.F., 1991. Did the breakout of Laurentia turn Gondwana inside out? Science 252, 1409–1412.

Jones, W.B., 1990. The Buem volcanic and associated sedimentary rocks, Ghana: a field and geochemical investigation. J. Afr. Earth Sci. 11, 373–383.

Jenner, G.A., Dunning, G.R., Malpas, J., Brown, M., Brace, T., 1991. Bay of Islands and Little Port complexes, revisited: age, geochemical and isotopic evidence confirm supra-subduction zone origin. Can. J. Earth Sci. 28, 135–162.

Junner, N.R., 1940. The geology of the gold coast and western Togoland. Gold Coast Geol. Surv. Bull. 11, 1–40.

Marchesi, C., Garrido, C.J., Godard, M., Proenza, J.A., Gervilla, F., Blanco-Moreno, J., 2006. Petrogenesis of highly depleted peridotites and gabbroic rocks from the Mayarí- Baracoa ophiolitic belt (eastern Cuba). Contrib. Mineral. Petrol. 151, 717–736.

Nude, P.M., Kwayisi, D., Taki, N.A., Kutu, J.M., Anani, C.Y., Banoeng-Yakubo, B., Asiedu, D.K., 2015. Petrography and chemical evidence for multi-stage emplacement of western Buem volcanic rocks in the Dahomeyide orogenic belt, Southeastern Ghana, West Africa. J. Afr. Earth Sci. 112, 314–327.

Osae, S., Asiedu, D.K., Benoeng-Yakubo, B., Koeberl, C., Dampare, S.B., 2006. Provenance and tectonic setting of the Late Proterozoic Buem sandstones of southeastern Ghana: evidence from Geochemistry and detrital modes. J. Afr. Earth Sci. 44, 85–96.

Rollinson, H.R., 1993. Using Geochemical Data: Evaluation, Presentation, Interpretation. Longman Group UK Limited, p. 352.

Rudnick, R., Gao, S., 2003. Composition of the continental crust. In: Rudnick, R.L. (Ed.), Treatise on Geochemistry, vol. 3. Elsevier-Pergamon Oxford, pp. 1–64.

Saunders, A.D., Norry, M.J., Tarney, J., 1988. Origin of MORB and chemically depleted mantle reservoirs: trace element constraints. J. Petrol. 415–445 (Special Lithosphere Issue).

Sun, S., McDonough, W., 1989. Chemical and isotopic systematics of oceanic basalts: implications for mantle composition and processes. Geol. Soc. Lond. Spec. Publ. 42, 313–345.

Tohver, E., D'Agrella-Filho, M.S., Trindale, R.I.F., 2006. Paleomagnetic record of Africa and South America for 1200–500 Ma interval, and evaluation of rodinia and Gondwana Assemblies. Precambrian Res. 147, 193–222.

Trompette, R., 1997. Neoproterozoic (600 Ma) aggregation of western Gondwana: a tentative scenario. Precambrian Res. 82, 101–112.

Villeneuve, M., Cornée, J.J., 1994. Structure, evolution and palaeogeography of the West African craton and bordering belts during the Neoproterozoic. Precambrian Res. 69, 307–326.

Villenenve, M., Dallmeyer, R.D., 1987. Geodynamic evolution of the mauritinide, bassaride and rokelide origens (West Africa). Precambrian Res. 37, 19–28.

Wilson, M., 1989. Igneous Petrogenesis. Unwin Hyman, London, p. 457.

Winchester, J., Floyd, P., 1977. Geochemical discrimination of different magma series and their differentiation products using immobile elements. Chem. Geol. 20, 325–343.

Winter, J., 2001. Introduction to Igneous and Metamorphic Petrology. Prentice Hall Upper Saddle River, New Jersey 07458, p. 796.

Wood, D.A., 1980. The application of a Th–Hf–Ta diagram to problems of tectonomagmatic classification and to establishing the nature of crustal contamination of basaltic lavas of the British Tertiary volcanic province. Earth Planet. Sci. Lett. 50, 11–30.

Zhou, M.F., Kennedy, A.K., Sun, M., Malpas, J., Lesher, C.M., 2002. Neoproterozoic arc-related mafic intrusions in the northern margin of South China: implications for accretion of Rodinia. J. Geol. 110, 611–618.

Zou, H.B., Zindler, A., Xu, X.S., Qu, Q., 2000. Major, trace element, and Nd, Sr and Pb isotope studies of Cenozoic basalts in SE China: mantle sources, regional variations, and tectonic significance. Chem. Geol. 171, 33–47.